



Investigation of the removal of sulfamethoxazole drug waste from aqueous solutions under the effect of zinc oxide/montmorillonite nanocomposite by photocatalytic ozonation process

Işıl Nihan Özyürek^a, Murat Kıranşan^{b,*}, Semra Karaca^{a,*}

^aDepartment of Chemistry, Faculty of Science, Atatürk University, 25240 Erzurum, Turkey, Tel. +90 442 2314435; Fax: +90 442 2360948; emails: isilnihan.ozyurek@atauni.edu.tr (I.N. Özyürek), skaraca@atauni.edu.tr (S. Karaca)

^bDepartment of Chemistry and Chemical Processing Technologies, Vocational School of Gumushane, University of Gumushane, 29100 Gümüşhane, Turkey, Tel. +90 456 2332915; Fax: +90 456 2331067; email: murat.kiransan@gumushane.edu.tr/murat_kiransan@yahoo.com

Received 5 December 2020; Accepted 3 October 2021

ABSTRACT

In this study, the synergistic effect of photocatalysis and ozonation processes to degrade the sulfamethoxazole (SMX), one antibiotic pharmaceutical compound, has been studied through the influence of main operational variables such as zinc oxide/montmorillonite (ZnO/MMT) dosage, SMX initial concentration, ozone flow rate, pH and the addition of organic and inorganic scavengers. Synthesized ZnO nanoparticles were immobilized on the montmorillonite surface to prepare ZnO/MMT catalyst as a photocatalyst. The catalyst was characterized by X-ray fluorescence, X-ray diffraction, scanning electron microscope, high-resolution transmission electron microscope and N₂ adsorption/desorption. The highest SMX degradation efficiency (80.84% for 30 min of reaction time) was obtained for the photocatalytic ozonation process compared to adsorption, single ozonation, catalytic ozonation, and photolysis. ZnO/MMT was more effective photocatalyst according to ZnO, indicating its usability as a promising photocatalyst for the removal of organic contaminants in aqueous solutions. The reduced degradation efficiency with the addition of organic and inorganic scavengers showed the important role of the photo-produced radicals and holes as well as direct ozonation in SMX degradation. A mechanism is also proposed for photocatalytic ozonation degradation by using the gas chromatography-mass spectroscopy (GC-MS) analysis method. Finally, several by-products were identified by GC-MS analysis, which allowed to depict a possible mechanism for the sulfamethoxazole degradation.

Keywords: Photocatalytic ozonation; Zinc oxide/montmorillonite nanocomposite; Sulfamethoxazole; Hydroxyl radical; Antibiotic

1. Introduction

The prominent increase in environmental pollution along with many different types of contaminants has revealed the growing demand for innovative water treatment technologies. Advanced oxidation processes (AOPs) for water purification and recovery have proved to be effective processes due to their higher capability to degrade permanent

toxic organic compounds, such as pharmaceuticals, personal care products, hormones, industrial additives and household chemicals whose existence even at low concentration can be deleterious for living organisms [1,2]. Pharmaceuticals and personal care products constitute the major class of contaminants due to their widespread usage and unknown biological and ecotoxicological effects. Some

* Corresponding authors.

of these pharmaceuticals may not be exactly removed or transformed during conventional wastewater treatment methods because they show high resistance to these methods. So, they are continuously discharged into the water environment, even if they are removed with this wastewater treatment [3,4]. In the advanced oxidation processes, the complete degradation and mineralization of such a type of contaminants in the water is possible through oxidation reactions with in situ generated the highly reactive, short-life and non-specific oxidizing species such as hydroxyl radical ($\cdot\text{OH}$), superoxide ($\cdot\text{O}_2^-$), ozonide ($\cdot\text{O}_3^-$), photogenerated electron-hole pairs [4,5]. Recently, it has been shown that the combination of ozone and heterogeneous photocatalysis under ultraviolet light (i.e., photocatalytic ozonation) can greatly improve pollutant degradation rates attained by single processes such as ozonation, photolytic ozonation, catalytic ozonation and photocatalysis and adsorption due to increased generation of reactive oxygen species (ROS) as a result of the synergistic effect between photocatalysis and ozonation [1,6,7]. Catalysts such as zinc oxide, iron oxide and titanium dioxide are the effective materials in the removal of metal ions, dyes, drugs by using photocatalytic degradation processes [8–11]. ZnO-montmorillonite nanocomposite and hybrid nanocomposites are the hybrid materials used in the removal of the wastes such as arsenic and methylcobalamin from wastewater [12–14].

The utilization of a suitable catalyst to achieve success in the photocatalytic ozonation process is an important factor. TiO_2 is the most widely used photocatalyst in photocatalytic ozonation processes due to its higher photocatalytic oxidation ability [15–17]. As an attractive alternative to TiO_2 for the photocatalytic ozonation processes under ultraviolet light radiation, ZnO as nontoxic material with a variety of nanostructures is preferred over TiO_2 for catalytic treatment of some environmental pollutants in wastewater due to its high quantum efficiency providing effective absorption of photons, low-cost and wide bandgap [18,19]. ZnO produces the electron having more negative potential in comparison with TiO_2 [20]. However, ZnO is not stable in the acidic environment and loses activity as aggregate at high loading. Moreover, its surface area is not so high for available adsorption [19]. The overcoming of this problem can be achieved by fixing the ZnO on stable inorganic support such as bentonite [20], activated carbon [21], sepiolite [22] and glass spiral [23]. Among them, clays and clay-based materials represent have an extremely high level of interest as the support material for immobilization of a variety of photocatalysts because they are cheap, chemically inert, resistant to deterioration, environmentally friendly, and widely available [20]. The montmorillonite as a catalyst and support material has attracted considerable attention in the last 10 y due to their thermal stability, exchangeable cations, swellable properties, nanoporous structure, appropriate surface morphology and large surface area which are beneficial to the activity of photocatalytic ozonation via enhancing adsorption, the determining step in the heterogeneous photodegradation reaction [22,24].

In the present study, montmorillonite K10 (MMT) clay was used as the matrix for the immobilization of ZnO. ZnO nanoparticles were synthesized and loaded on the surface of montmorillonite K10 (MMT) via sol-gel method for

degradation of sulfamethoxazole as the target pollutant. The activity of this MMT-supported ZnO was evaluated in the oxidation of sulfamethoxazole. For this aim, the combination of heterogeneous photocatalysis and ozonation have been applied to remove the sulfamethoxazole from aqueous solutions and compared with other systems such as single ozonation, photolytic ozonation, catalytic ozonation, photocatalysis and adsorption. The effect of various parameters such as catalyst amount, initial pharmaceutical concentration, solution pH, presence of scavengers is investigated and optimum conditions for the degradation are identified.

2. Material and methods

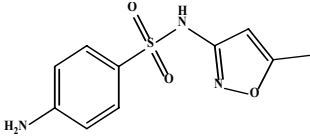
2.1. Materials

Sulfamethoxazole, 4-amino-N-(5-methylisoxazol-3-yl) benzenesulfonamide, ($\text{C}_{10}\text{H}_{11}\text{N}_3\text{O}_3\text{S}$) chosen as model organic pollutants, was provided by Sigma-Aldrich Co., (Sigma-Aldrich, St. Louis, MO, USA), and dissolved in distilled water. The characteristics and chemical structure of sulfamethoxazole are shown in Table 1. ZnCl_2 , HCl and NaOH were bought from Merck Co., (Germany) and montmorillonite K10 (MMT) from Sigma-Aldrich Co., (USA) which consists of SiO_2 , Al_2O_3 , Fe_2O_3 , MgO, CaO, Na_2O , and K_2O with 66.9, 13.8, 2.8, 1.6, 0.3, 0.2 and 1.7 wt.% respectively. The cation exchange capacity of the MMT was 120 meq/100 g, which was determined using the Methylene blue method [25]. All of the other chemicals were purchased from Sigma-Aldrich Co., (USA) and they were analytical grade purity. All of them were used as received in all experiments. Deionized water was used to prepare aqueous solutions throughout the investigation.

2.2. Catalyst synthesis and characterization

To prepare zinc oxide/montmorillonite (ZnO/MMT) nanocomposite, the synthesized ZnO nanoparticles was immobilized on the surface of MMT as published elsewhere [26]. To examine the surface morphology of the MMT particles and ZnO/MMT catalyst, scanning electron microscope (SEM) model (TESCAN MIRA3 FEG-SEM, Czech) and high-resolution transmission electron microscope (HR-TEM) model JEM-2100F, JEOL (Japan) operated at 100 k were used. The X-ray diffraction (XRD) patterns of pure MMT and ZnO/MMT composite were collected by PANalytical X'Pert PRO diffractometer (Germany) with Cu K_α radiation ($\lambda = 0.15406$ nm) at 45 kV and 40 mA in the range from 3° to 70° of 2θ . The chemical composition of the MMT and synthesized ZnO/MMT was assessed by X-ray fluorescence (XRF) (Rigaku ZSX Primus II, Japan). Textural properties of the MMT, ZnO and ZnO/MMT samples were determined from N_2 adsorption-desorption isotherms at 77 K on a Gemini 2385 nitrogen adsorption apparatus (Micromeritics Instruments, USA) and their surface areas and pore size distributions were analyzed using the Brunauer-Emmett-Teller (BET) and Barrett-Joyner-Halenda (BJH) method, respectively. Prior to the nitrogen physisorption measurements, the samples were degassed at 105°C for 15 h in order to remove physisorbed water without any effect on the textural properties of investigated samples.

Table 1
Characteristics of the sulfamethoxazole (SMX)

Chemical structure	Molecular formula	M_w (g mol ⁻¹)	λ_{max} (nm)	Therapeutic group	Solubility in water (mg mL ⁻¹)
	C ₁₀ H ₁₁ N ₃ O ₃ S	253.27	265	Antibiotic	<1

2.3. Experimental procedure

Photocatalytic ozonation experiments were carried out in a 900 mL capacity cylindrical glass photoreactor containing UV-A lamp of 8W (Sylvania, Japan) placed inside a quartz tube within the reactor, inlet for ozone and outlet for the non-absorbed ozone gas. A schematic diagram of the reactor is represented in Fig. 1. The outer surface of the reactor was sealed with aluminum foil to avoid exposure to sunlight. The reactor contents were stirred continuously with a magnetic stirrer. The ozone gas was generated using the TOGC2, Triogen (Scotland) ozone generator, and the produced ozone was continuously bubbled into the reactor through a diffuser settled at the bottom of the reactor.

In a typical approach, 500 mL of sulfamethoxazole solution with a known initial concentration containing the desired amount of catalyst was fed to the reactor. The experiments were carried out at the natural pH (pH = 5) and at the ozone gas flow rate of 2 L h⁻¹ (except for the experiments in which the effect of solution pH and gas flow rate were examined). At desired time intervals, samples of 5 mL were taken and a small amount of sodium sulfite was added to the samples to exterminate any progress of ozone or hydroxyl radical oxidation before the analytical

determination of sulfamethoxazole by using a UV-Vis spectrophotometer. After the centrifugation of the samples, the remaining sulfamethoxazole concentration was determined using Varian Cary 100 UV-Vis spectrophotometer (Australia) at a maximum wavelength of 265 nm.

UV-Vis spectral changes of sulfamethoxazole as a function time during photocatalytic ozonation process in the presence of initial 20 mg L⁻¹ sulfamethoxazole (SMX) for 0.1 g L⁻¹ ZnO/MMT at pH of 5 under ozone gas flow rate of 2 L h⁻¹ and UV-A irradiation and the results are illustrated in Fig. 2. The intensity of the maximum peak located at the wavelength of 265 nm reduced depending on the reaction time, and it almost disappeared after the reaction time of 15 min. This result obviously reveals the SMX degradation on the ZnO/MMT surface via the photocatalytic ozonation method. Complete degradation of SMX was carried out after 30 min in the optimized conditions.

2.4. Analysis of sulfamethoxazole degradation products with gas chromatography-mass spectroscopy

Gas chromatography-mass spectroscopy (GC-MS) analysis was carried out to determine intermediate products of sulfamethoxazole degradation by photocatalytic

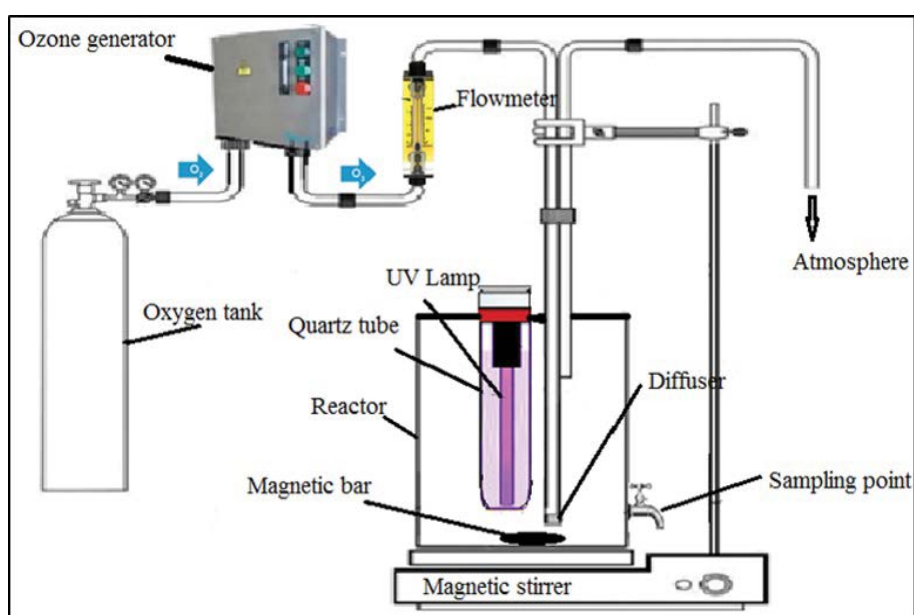


Fig. 1. Schematic representation of the reactor used for photocatalytic ozonation process.

ozonation. 1 L sulfamethoxazole solution was treated with photocatalytic ozonation for 15 min and organic intermediates were extracted three times with 30 mL of diethyl ether. The resulting organic solution was held to evaporate the organic solvent and the remaining solid was dissolved in 100 μL of N,O-bis(trimethylsilyl) acetamide, heating at 60°C and stirring for 10 min. The products obtained were analyzed by GC-MS device (Agilent 6890 Gas Chromatography and 5973 Mass Spectrometer, Palo Alto, Canada).

2.5. Thermogravimetric analysis/Differential thermogravimetric/Differential thermal analysis studies

The thermal degradation process of ZnO and ZnO/MMT nanocomposite were investigated using thermogravimetric analysis (TGA)/Differential thermogravimetric (DTG)/differential thermal analysis (DTA) thermogravimetric analysis (HITACHI STA7300, Japan) under nitrogen atmosphere from 30°C to 900°C with a heating rate of 10°C min⁻¹.

3. Results and discussion

3.1. Structural characterization of the MMT and ZnO/MMT nanocomposite

The obtained chemical composition results of pure MMT and ZnO/MMT nanocomposite by using an XRF spectrometer are given in Table 2. When these results are compared with each other, it is shown that the presence of ZnO in significant amounts in the composite structure, such as 48% is evident. On the other hand, SiO₂ amount of 66.90% and Al₂O₃ amount of 13.80% in MMT were reduced to 36.30% and 10.30, respectively in the ZnO/MMT structure. This result clearly shows that the incorporation of ZnO between the interlayer galleries of MMT and hybridization with MMT.

Fig. 3 indicates X-ray diffraction patterns documented for MMT, pure ZnO and ZnO/MMT nanoparticles. In Fig. 3a, the observed peaks at 8.5°, 19.84°, 26.65°,

34.93°, 61.66° of 2 θ values are specific peaks for MMT [27,28]. The peak at 2 θ of 26.65° of the XRD pattern of MMT (JCPDS Card 35-0652) shown in Fig. 3a, corresponds to the interlayer spacing of this clay [29,30]. After the immobilization of ZnO onto the MMT surface, the d₀₀₁ peak at 2 θ = 8.5 where the intercalation reactions in the clay structure occur, shifted towards to lower angle side compared with pure MMT, indicating the enlargement of the basal spacing of the MMT as a result of the interaction between MMT and ZnO nanoparticles (Fig. 3c). Moreover, the new reflections were also seen (Fig. 3b and c) in the XRD pattern of pure ZnO and ZnO/MMT at 2 θ of 31.71° (100), 34.41° (002), 36.21° (101), 47.51° (102), 56.61° (110), 63° (103), 66.08° (200), 68° (112) and 68.28° (201) which are characteristics ZnO peaks (JCPDS Card 36-1451) [29,30]. The reflection at 2 θ = 31.71° could be a reflection of ZnO in the hexagonal wurtzite crystal structure (Fig. 3b). Based on these results, it can be said that ZnO/MMT nanocomposite was formed through the synthesis of ZnO nanoparticles on the MMT. Using the Debye–Scherrer equation [31], the crystallite size of ZnO in ZnO/MMT was calculated to be about 25 nm.

To investigate the surface morphology of the MMT and ZnO/MMT particles, SEM and HR-TEM analysis were used and the collected results are presented in Figs. 4 and 5. As can be seen in Fig. 4a, the SEM image of MMT exhibited a fairly porous structure and heterogeneous surface morphology with cracks and phase separations. Compared to the pure MMT, the presence of flower-like ZnO particles on the MMT (Fig. 4b) approved successful immobilization of ZnO into the MMT surface. Fig. 4c shows that in the energy-dispersive X-ray (EDS) spectrum of MMT, C (carbon) 21.51%, Si (Silicon) 36.11%, O (oxygen) 35.02% and Al (aluminium) 6.66% by weight. Fig. 4d shows that Zn (zinc) 48.60%, C (carbon) 3.3%, Si (silicon) 12.0%, O (oxygen) 24.3% and Al (aluminum) 3.1% by weight in the EDS spectrum of ZnO/MMT nanocomposite. As seen in the EDS spectrum of ZnO/MMT, the high amount of Zn by weight and the decrease of other components (C, Si, O, Al) indicate that ZnO particles are immobilized between the layers of MMT [32].

The obtained HR-TEM images for pure MMT and ZnO/MMT seem to support this idea (Fig. 5a and b). In Fig. 5b, plate-like ZnO particles in nm size on porous MMT surface are obvious. HR-TEM images show that the ZnO/

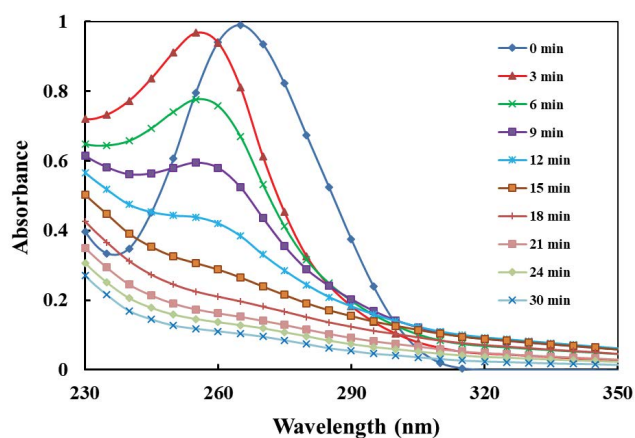


Fig. 2. The changes in the absorption spectra of 20 mg L⁻¹ of sulfamethoxazole during different treatment time. Experimental conditions: [ZnO/MMT]: 0.1 g L⁻¹; [SMX]₀: 20 mg L⁻¹; ozone gas inlet flow rate: 2 L h⁻¹; pH = 5.

Table 2
Chemical composition of MMT and ZnO/MMT samples

Compound (%)	MMT	ZnO/MMT
ZnO	–	48.01
SiO ₂	66.90	36.30
Al ₂ O ₃	13.80	10.30
Fe ₂ O ₃	2.75	2.23
MgO	1.58	0.92
CaO	0.29	0.22
Na ₂ O	0.15	–
K ₂ O	1.65	1.23
Other	12.88	0.79

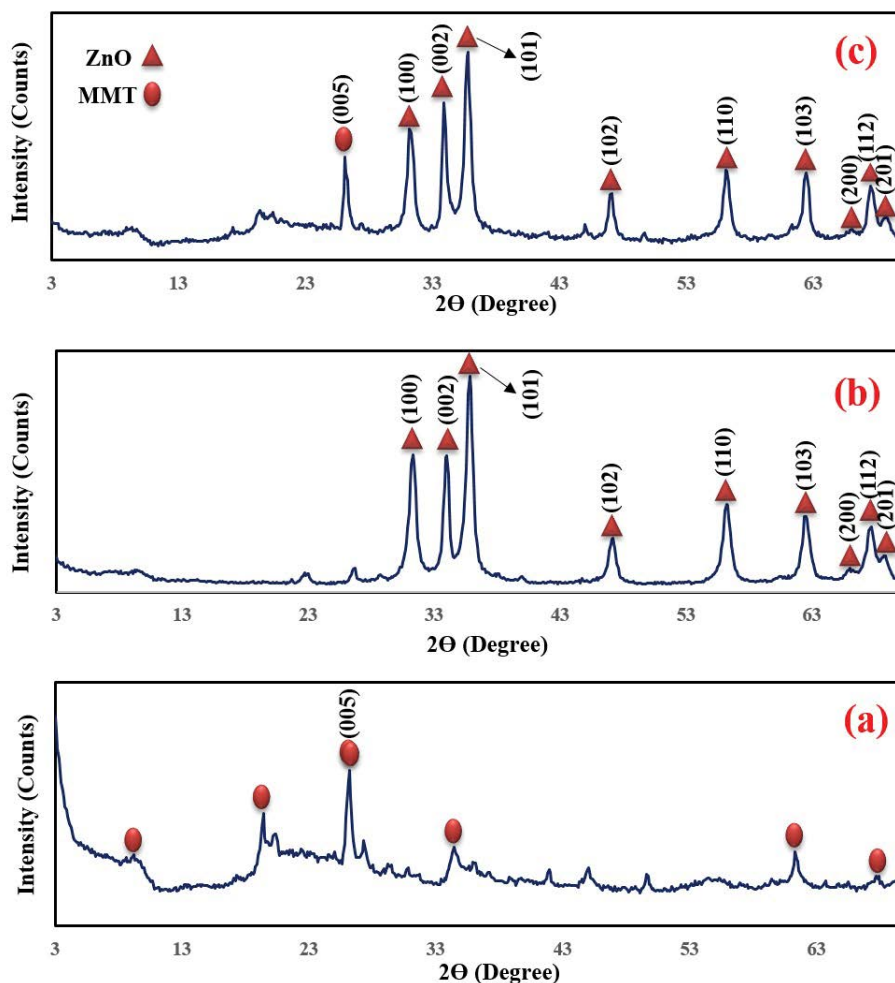


Fig. 3. XRD patterns for (a) raw MMT, (b) pure ZnO and (c) ZnO/MMT nanocomposite.

MMT particles are within the nanoscale. According to the HR-TEM analysis results, it was clearly understood that the used method in this study was a reliable and convenient method for the preparation of ZnO/MMT nanocomposites with predictable results.

Fig. 6 shows adsorption–desorption isotherms of N_2 at 77 K for MMT and synthesized ZnO and ZnO/MMT. As can be seen from the figure, the MMT sample exhibited type II isotherm with hysteresis loops exhibiting the strong interaction between adsorbent and adsorbate molecules and a mesoporous texture with a uniform pore size distribution. The isotherm for pristine MMT presents a H4 typed hysteresis loop, indicating that the sample has narrow slit pore (Fig. 6c) [33]. The isotherms for ZnO and ZnO/MMT exhibited a typical type IV curve with hysteresis loops according to the IUPAC classification, corresponding to mesoporous materials and associated with capillary condensation [34]. Both ZnO and ZnO/MMT nanocomposites have a H3 type hysteresis loop with a lamellar pore structure and disordered slit and wedge shape (Fig. 6a and b) [35]. It is considered that the location of the inflection point of P/P^0 relates to a diameter in the mesopore range, and the uniformity of the mesopore size distribution has

been shown with the sharpness step [36]. Capillary condensation in MMT started approximately at $P/P^0 = 0.40$ while the beginning of this action was about at P/P^0 of 0.25 for ZnO and ZnO/MMT nanocomposite. Compared with MMT, shifting of the inflection point, which is the beginning of capillary condensation, in ZnO/MMT nanocomposite to lower P/P^0 range can be attributed to ZnO incorporation into MMT interlayer galleries [37].

The pore size distributions of the samples were calculated from the BJH adsorption branch of the isotherm (Fig. 7). The average pore size radius of the MMT, ZnO and ZnO/MMT samples was estimated to be 3.17, 14.96 and 5.45 nm, respectively. Additionally, the BET surface areas for the MMT, ZnO and ZnO/MMT were 279.27, 38.22 and 70.54 $m^2 g^{-1}$, respectively. The average pore size of MMT increased and the specific surface area decreased with the loading of ZnO, which may be caused by a collapsing of some part of the MMT porous structure as a result of the incorporation of ZnO crystallite between the layers of MMT [38] as shown in Fig. 7.

After heating the ZnO/MMT nanocomposite up to 400°C, the mass loss occurred. The decrease in the DTA curve at 400°C confirms this transition. A decrease in the DTA curve

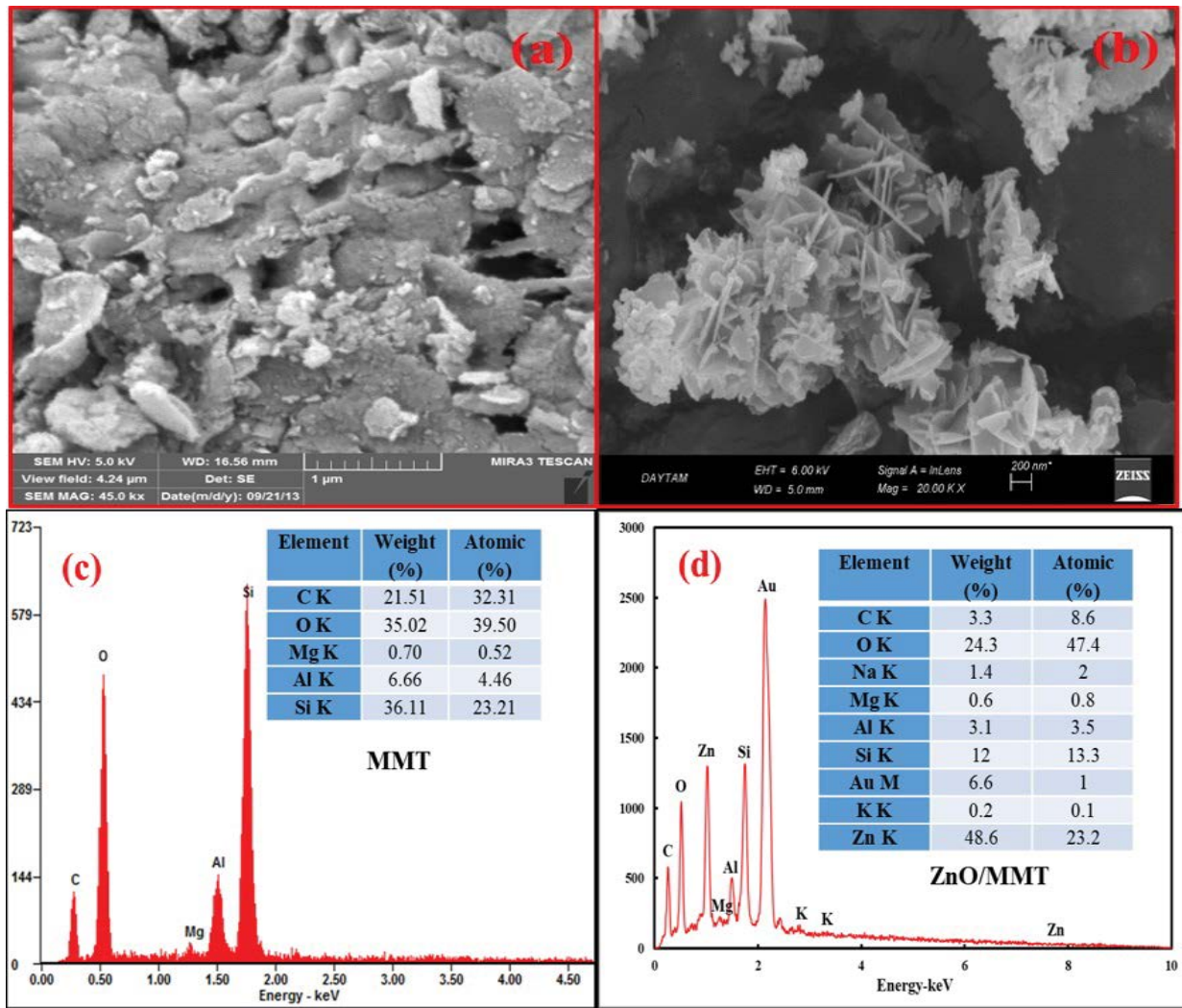


Fig. 4. SEM images of (a) raw MMT, (b) ZnO/MMT nanocomposite and EDS spectra of (c) raw MMT, (d) ZnO/MMT nanocomposite.

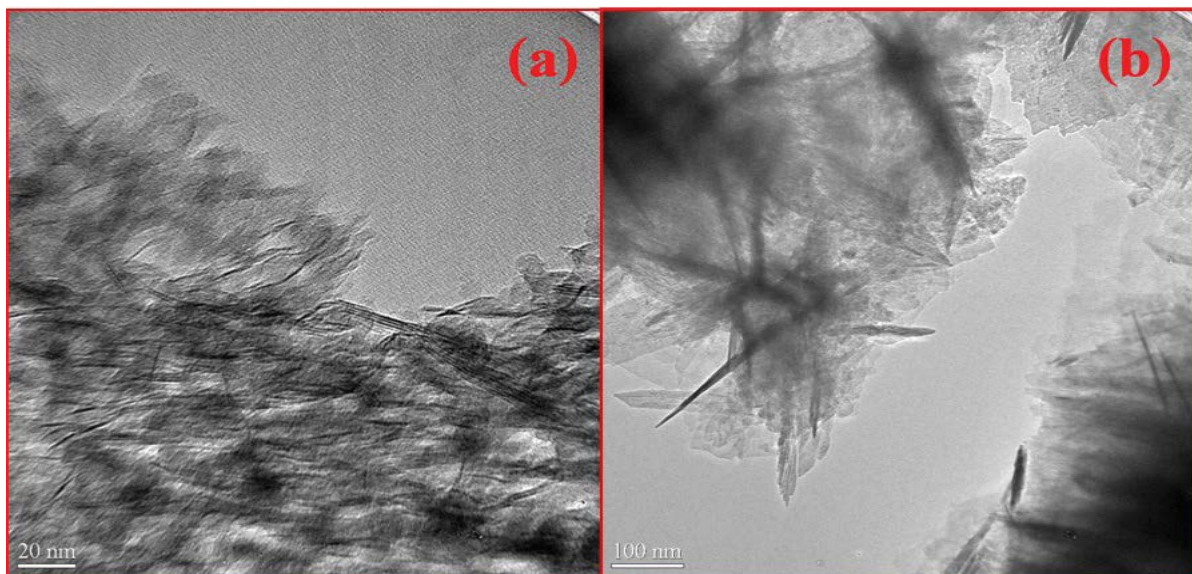


Fig. 5. HR-TEM images of (a) raw MMT and (b) ZnO/MMT nanocomposite

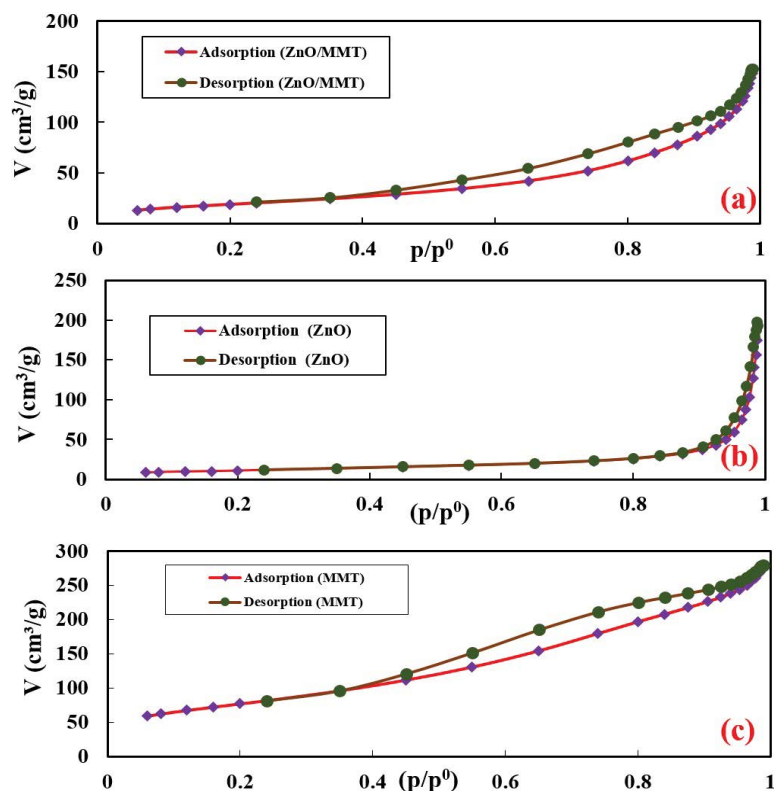


Fig. 6. Nitrogen adsorption–desorption isotherms of (a) ZnO/MMT nanocomposites, (b) ZnO nanoparticles and (c) MMT.

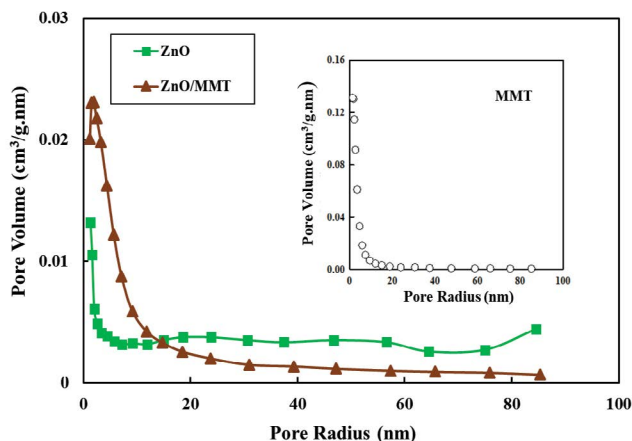


Fig. 7. BJH pore size distribution of the samples.

of ZnO/MMT nanocomposite was observed from 400°C to 800°C. The decrease in the TG curve of the nanocomposite confirms the DTA curve. DTA/TGA/DTG analysis results of ZnO and ZnO/MMT as shown in Fig. 8 [39].

3.2. Comparison of different processes on the sulfamethoxazole degradation efficiency

In order to evaluate the degradation efficiency of sulfamethoxazole by different processes, some preliminary experimental series were conducted in the investigated systems such as adsorption (ZnO/MMT), ozonation (O_3),

photolysis (UVA), catalytic ozonation (ZnO/MMT- O_3), photocatalysis (ZnO/MMT-UVA), and photocatalytic ozonation (ZnO/MMT-UVA- O_3 and ZnO/UVA- O_3). The results are given in Fig. 9. The values of initial sulfamethoxazole concentration, catalyst dosage, gas flow rate and pH were constant as 20 mg L⁻¹, 0.1 g L⁻¹, 2 L h⁻¹ and pH = 5.0 respectively (Fig. 9).

As presented in Fig. 9, the degradation of SMX was low (17.64%) by direct photolysis under UV-A irradiation (315–400 nm) exhibiting the inefficiency of photolysis in the degradation of SMX. This phenomenon can be explained that the photocatalyst absorbing the emitted photons by the UV light source and/or the value of photon energy released by UV irradiation is not sufficient to break bonds in SMX [40–42]. Hence, SMX did not degrade by the photolysis process. Similar results were observed by previous researchers that have examined the degradation of phenazopyridine hydrochloride, sulfamethoxazole and perfluorooctanoic acid by photolysis [40–42]. SMX removal was only 23.14% in the adsorption process, indicating the contribution of adsorption onto ZnO/MMT surface is not considered in SMX degradation. Fig. 9 demonstrates that the degradation efficiency of SMX by photocatalysis process was rather slow and it was carried out within 30 min as 27.92%. According to this, it was understood that the complete degradation of organic pollutants needs more reaction times due to probably the rapid recombination of the produced e^-/h^+ pairs on the photocatalyst surface in the presence of oxygen resulting in a reduction in the amount of generated hydroxyl radicals [41].

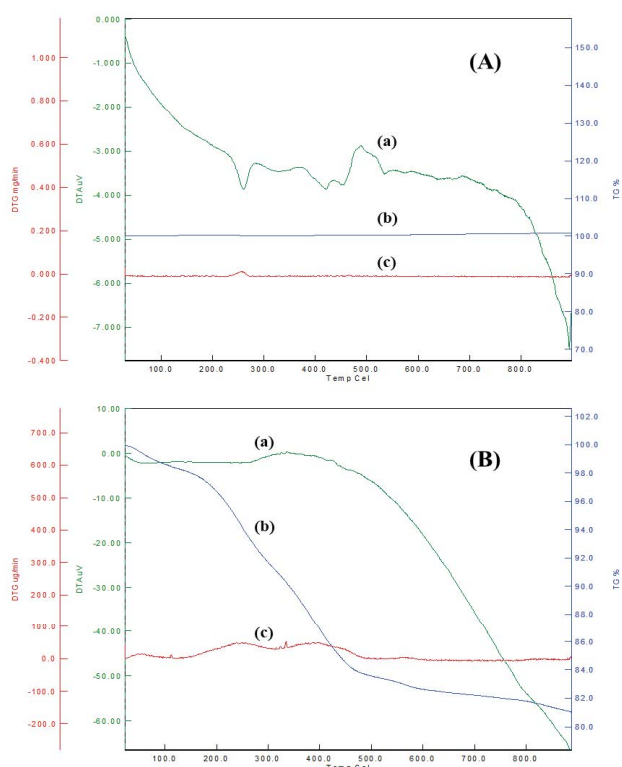


Fig. 8. (A) Analysis of ZnO (a) DTA, (b) TGA, (c) DTG; (B) Analysis of ZnO/MMT nanocomposite (a) DTA, (b) TGA, (c) DTG.

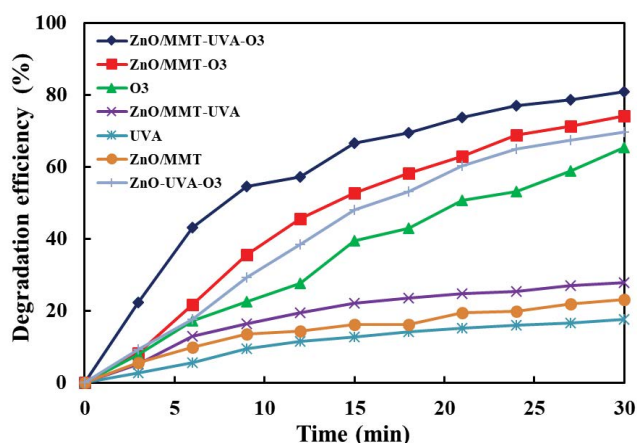


Fig. 9. Comparison of different processes in the sulfamethoxazole degradation as a function of time. Experimental conditions: [Catalyst]: 0.1 g L⁻¹; [SMX]₀: 20 mg L⁻¹; pH = 5.

The degradation efficiency of the SMX is 65.39% after 30 min of reaction using a single ozonation process, which is importantly higher than that of photocatalytic oxidation. As discussed in the literature, the oxidation of organic species by ozone without catalyst takes place principally in the liquid phase through both direct and indirect mechanism processes where the produced hydroxyl radicals by ozone decomposition react with pollutant [41,43].

As increasing the solution pH, especially in alkaline conditions, the ratio of indirect oxidation to direct oxidation rises. Hence, pollutant removal efficiency increases due to the higher reactivity of hydroxyl radicals compared to ozone [43]. Direct reaction of ozone is great of importance in acid and neutral media for organic pollutants in a solution that react very fast with ozone. Therefore, it can be said that the electrophilic attack of ozone may take place at the aromatic ring and S=O double bond of SMX under applied conditions in this study (pH = 5) [44,45]. As can be seen in Fig. 9, with the addition of ZnO/MMT as a heterogeneous photocatalyst to the ozonation system, the degradation efficiency of SMX improved compared with a single ozonation system (74.05% at 30 min). This may be due to the implementation of the heterogeneous catalytic ozonation on the surface of the ZnO/MMT surface. When the photocatalyst is added to the ozonation system, as opposed to ozonation alone, efficient production of hydroxyl radicals occurs at a low pH value which results in an improvement in the SMX degradation efficiency [44,46]. For the photocatalysis and ozonation combined system, SMX degradation efficiency was carried out as 69.6% and 80.84% for ZnO and ZnO/MMT catalysts, respectively within 30 min reaction time, which suggested the existence of synergistic effect between photocatalysis and ozonation (Fig. 9). It was reported that with the addition of ozone to the photocatalytic system, the quantum efficiency of photocatalysis is improved which results in the abundantly photoproducted holes participating in the reaction with SMX rather than recombining with photo-generated electrons [42]. In the photocatalytic ozonation processes, the adsorption of both pollutants and ozone on the surface of the photocatalyst is considered as a first step of the surface degradation process. Afterwards, adsorbed molecules may react with each other (direct pathway) or with the photoproducted electrons (indirect pathway) in adsorbed phase [44]. On the other hand, it can be suggested as a second mechanism that the adsorbed pollutant molecules on the surface of the catalyst may react with dissolved molecular ozone [44]. Ozone which has a higher absorption coefficient, absorbs the UV radiation with wavelength below 320 nm, by generating additional hydroxyl radicals and other oxidants, with enhanced degradation efficiency [44,45]. [Eqs. (1)–(4)].



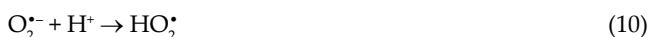
All possible reaction steps during the production of hydroxyl radicals can be summarized as follows [40–47]. One of them, under UV irradiation, absorption of the photons with the higher energy of ZnO nanoparticles band gap leads to oxidant positive hole formation on the valence band and electron migration to the conduction band as shown in Eq. (5) [40–47].



The generation of hydroxyl radicals is possible through ozonide radical formation in the adsorption layer by means of direct electron transfer from ZnO under UV light to the ozone molecule [41–43] [Eqs. (6)–(8)].



Superoxide anion radical forms with the electron transfer from ZnO to the oxygen molecule which then reacts with ozone to produce hydroxyl radicals through the formation of an ozonide radical [Eqs. (6) and (9)–(11)] [46];



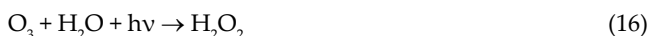
Then, the ozonide radical rapidly reacts with H^+ to produce HO_3^{\bullet} [Eq. (12)], which in turn generates molecular oxygen and $\bullet\text{OH}$ radicals [Eq. (13)] [43].



Photo-generated positive holes react with adsorbed water molecules to generate hydroxyl radicals by Eqs. (14)–(15) [46];



Hydrogen peroxide as intermediates produces in the existence of ozone and under UV radiation and then hydroxyl radicals forms according to Eqs. (16)–(22) [43–45].



According to Eq. (20), the produced superoxide anion ($\text{O}_2^{\bullet-}$ from HO_2^{\bullet}) dissociation ($\text{pK}_a = 4.8$) at $\text{pH} = 5$ which is the pH value in this study, improved the synergistic effect

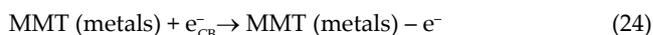
of the photocatalytic ozonation process by participating in SMX degradation.

Also, dissolved ozone can easily accept the electrons in the conduction band [Eq. (23)].

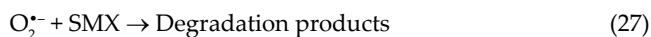
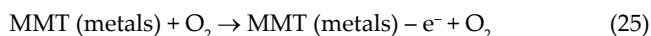


So, the recombination of the positive holes and negative electron pairs is suppressed. Finally, the increase in the number of produced radicals leads to the acceleration in the degradation efficiency [45].

The degradation efficiency of SMX by photocatalytic ozonation in the ZnO/MMT- O_3 -UVA system (80.84%) was higher than that of the ZnO- O_3 -UVA system (69.6%) (Fig. 9). The improvement in the degradation efficiency of SMX by the immobilization of ZnO nanoparticles on the surface of MMT can be attributed to the trapping ability of metals the electrons in the conduction band (CB) of ZnO and the efficient separation of e^-/h^+ pairs which play a key role in the development of the photocatalytic activity of the ZnO/MMT [48]. Under UV irradiation, photo-generated electrons and holes occur on the photocatalyst surface [Eq. (5)]. Photogenerated electrons over ZnO are received by the possible d-orbits vacant cations in the galleries of MMT and/or charges can directly play a role in reduction and oxidation processes [48]. Thus, the recombination of the photogenerated electron-hole pairs is inhibited. This reaction can be given as follows:



Moreover, the recombination of electron-hole suppresses through the reactions between the MMT and the superoxide species [49] [Eqs. (25)–(27)]. So, the degradation efficiency of SMX is increased.



On the other hand, ZnO/MMT catalyst has a higher surface area as a result of ZnO delamination in the interlayer galleries of MMT. Consequently, the more photocatalytic reaction active sites occur on the catalyst surface leading to efficiently light capture, more adsorption and the improvement in the SMX degradation. SMX degradation pathways in this study through oxidation by hydroxyl radicals, photo-excited holes and superoxide ion radicals and direct ozonation were summarized during photocatalytic ozonation in Fig. 10.

To confirm the synergistic effect between photocatalysis and ozonation processes in the photocatalytic ozonation of SMX by using ZnO/MMT catalyst, the synergy factor was calculated. For this, pseudo-first-order rate constants for both combined and individual ozonation and photocatalytic oxidation processes were calculated according to Eq. (28).

$$\text{Synergy factor} = \frac{k_{\text{app}}^{\text{photocatalytic ozonation}}}{k_{\text{app}}^{\text{ozonation}} + k_{\text{app}}^{\text{photocatalytic oxidation}}} \quad (28)$$

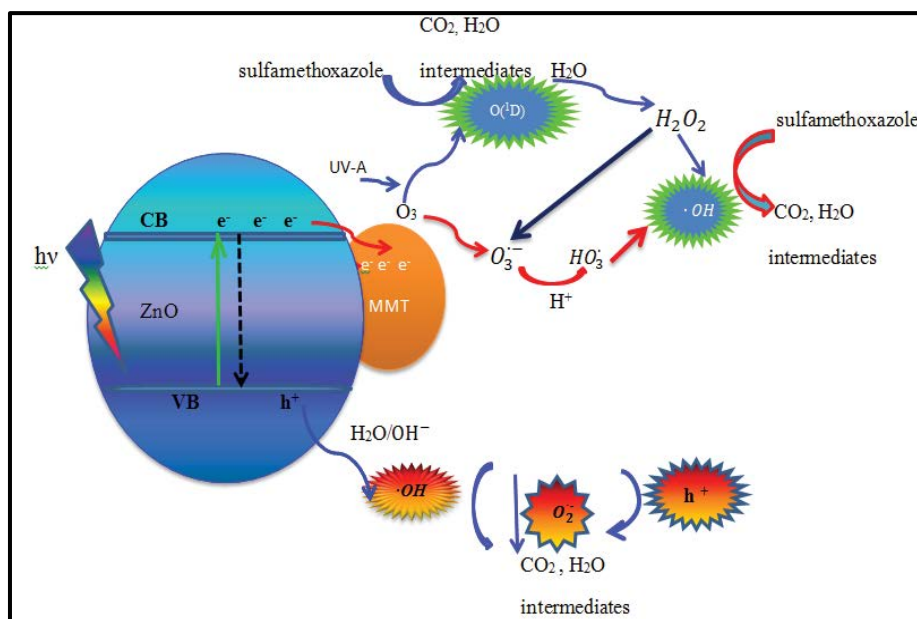


Fig. 10. Schematic representation of SMX degradation during photocatalytic ozonation with ZnO/MMT as photocatalyst.

The apparent pseudo-first-order rate constants (k_{app}) for photocatalytic ozonation, ozonation and photocatalytic processes were calculated based on Eq. (29) which was found to be 0.0529, 0.0352 and 0.0091 min^{-1} , respectively.

$$\ln \frac{A_0}{A} = k_{app} t \quad (29)$$

The synergy factor was found to be 1.19 which is bigger than 1. These results support a synergistic effect between photocatalysis and ozonation in this study under the worked conditions (catalyst dosage of 0.1 g L^{-1} , the initial SMX concentration of 20 mg L^{-1} , ozone flow rate of 2 L h^{-1} and $\text{pH} = 5$), rather than additive behavior in the integrated process.

Consequently, it was understood that the synergistic effects between photocatalysis and ozonation by using ZnO/MMT photocatalyst were efficiently increased the SMX degradation. Based on the above results it can be said that the treatment of wastewaters involving the pharmaceuticals by photocatalytic ozonation process under UV light irradiation accompanied with ZnO/MMT as an excellent photocatalyst is a promising way. And also, this system should be a low-cost, efficient, and nontoxic technology for the removal of similar contaminants in wastewaters.

3.3. Effect of catalyst amount

To determine the optimum catalyst dosage, a series of the photocatalytic ozonation experiments were carried out by varying the amount of catalyst from 0.075 to 0.25 g L^{-1} at a constant SMX concentration of 20 mg L^{-1} , gas inlet flow rate of 2 L h^{-1} and at natural pH ($\text{pH} = 5$). The obtained results are illustrated in Fig. 11. As depicted in Fig. 11, the degradation efficiency of SMX in photocatalytic ozonation increased with catalyst loading up to 0.1 g L^{-1} and above this loading

reduced. Many factors play a role in catalyst loading for pollutant degradation efficiencies such as the catalyst surface and absorption of light by the catalyst molecules [50–52]. As the catalyst amount is increased, the degradation efficiency is increased by up to 0.1 g L^{-1} due to the increase in the number of available active sites on the catalyst surface.

But, the higher catalyst loadings may not be beneficial both in terms of increased aggregation tendency of catalyst particles and the enhanced light scattering phenomena leading to the reduced irradiation field. Moreover; the increase in turbidity of the solution reduces the light penetration through the solution [50–52]. As a result, SMX degradation efficiency is decreased. Taking into account all the results, a catalyst dosage of 0.1 g L^{-1} were selected as the optimal catalyst amount in this study.

3.4. Effect of initial SMX concentration

The effect of initial SMX concentration on the degradation efficiency during photocatalytic ozonation process was performed by varying the initial SMX concentration from 5 to 40 mg L^{-1} with constant catalyst amount (0.1 g L^{-1}), gas flow rate (2 L h^{-1}), at natural pH ($\text{pH} = 5$) and the results presented in Fig. 12. As seen in Fig. 12, the removal efficiency of the SMX was significantly changed by the pharmaceutical concentration. The degradation of SMX relates to the formation of reactive oxygen species which is the critical species in the degradation process. Under constant conditions, if the ozone inlet flow rate and catalyst amount are constant, the dissolved ozone concentration, catalyst surface and the produced hydroxyl radicals remain constant. It should be noted that by enhancing SMX concentration, the requirement of reactive oxygen species needed to degrade the molecules of the pharmaceutical increases. However, the number of the generated reactive oxygen species attacking SMX molecules does not

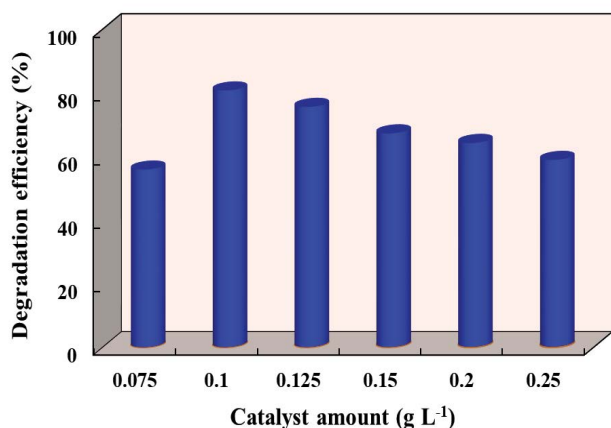


Fig. 11. Effect of ZnO/MMT amount on the degradation efficiency of sulfamethoxazole at the reaction time of 30 min. Experimental conditions: $[SMX]_0$: 20 mg L⁻¹; ozone gas inlet flow rate: 2 L h⁻¹; pH = 5.

change for an applied ozone flow rate and time. Therefore, the concentration of the produced oxidative species was not enough to degrade the high concentration of SMX. Consequently, the removal efficiency of SMX decreases with an increase in SMX concentration [50,52].

On the other hand, light absorption by catalyst particles is very important in photocatalytic reactions, due to the production of electron-hole pairs by light energy. By regarding the Lambert-Beer law, when the initial pollutant concentration is increased, the reduced input path length of photons to the solution leads to the lower photon adsorption on photocatalyst particles and reduced reactive oxygen species production. This demonstrates that the degradation of SMX reduces considerably with an increase in pollutant concentration [50,52].

3.5. Effect of ozone inlet flow rate

To demonstrate the effect of ozone dosage on the removal efficiency of SMX, various ozone gas inlet flow rates from 1 to 5 L h⁻¹ were used for degradation of SMX during photocatalytic ozonation process with and without ZnO/MMT catalyst. Other operational parameters, involving ZnO/MMT dosage, initial solution pH and initial SMX concentration, were kept constant at 0.1 g L⁻¹, 5.0 and 20 mg L⁻¹, respectively.

The results are given in Figs. 13 and 14. The obtained degradation rate constants, with and without ZnO/MMT catalyst along with their corresponding regression coefficients, are presented in Table 3. As can be seen from the figures, the increase of gas flow rate leads to an increase in the degradation efficiency and rate of SMX in both of media indicating the importance of ozone mass transfer from gas to liquid phase or catalyst surface. However, this trend was more low at high ozone concentrations in O₃/SMX system because ozone is a poorly soluble gas in water and ozone saturated water solution occurs even at the low flow rates of ozone [53,54]. When the obtained rate constants are compared with each other, it is shown that the increase in

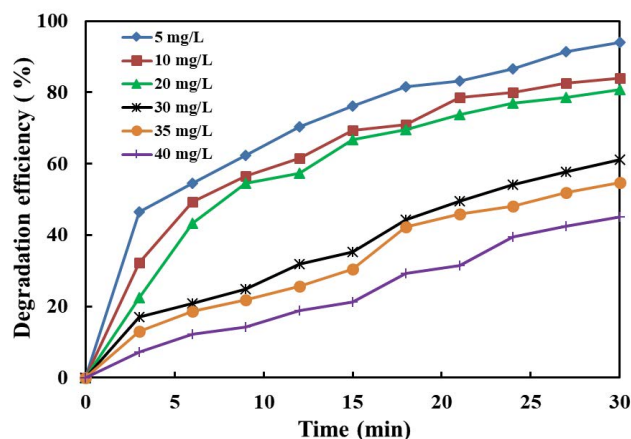


Fig. 12. Effect of initial sulfamethoxazole concentration on the degradation efficiency by ZnO/MMT under photocatalytic ozonation process. Experimental conditions: $[ZnO/MMT]_0$: 0.1 g L⁻¹; ozone gas inlet flow rate: 2 L h⁻¹; pH = 5.

rate constants by enhancing gas flow rate in the photocatalytic ozonation process is more in the ozonation process (Table 3). This result implies that the internal diffusion and the mass transfer resistance to the solid surface are more effective than the gas-liquid mass transfer resistance. On the other hand, it may be said that the proposed mechanism for photocatalytic ozonation is dominantly simultaneous adsorption of ozone and pollutants molecules on the catalyst surface followed by the reaction in the adsorbed phase through by direct or indirect pathway to produce reactive oxygen species (ROS) and/or the continuous generation of the radicals by dissolved ozone in water that is transferred to the catalyst surface as well as pollutant adsorption on the catalyst surface [55].

As the gas flow rate is increased, the improvement of the degradation efficiency of SMX is attributable to an increase in the amount of reactive oxygen species (ROS), particularly hydroxyl radicals. As seen from Figs. 13 and 14, an increase of the ozone gas flow rate from 1 to 2 L h⁻¹ yields higher SMX degradation efficiency and rates while a further enhancement of ozone concentration does not have any significant effect. Therefore, the gas flow rate of 2 L h⁻¹ was kept constant at all experiments.

3.6. Effect of initial solution pH

pH of the solution is one of the most prominent variables affecting the photocatalytic ozonation process because it determines the surface charge distribution of the photocatalyst and pollutant, the production of oxidizing species as well as reaction rate on the photocatalyst surface [56]. Therefore, the effect of initial solution pH on the SMX degradation during the photocatalytic ozonation process was studied in the pH range of 3–11 and the results are exhibited in Fig. 15a and b. It is observed that the degradation rate was highest at pH = 3, and then decreased with an increase in pH. The zpc value (zero-point charge) of ZnO/MMT is 8.4 at pH < 8.4. According to this, the surface of ZnO/MMT is positively charged at pH < 8.4

whereas it is negatively charged at $\text{pH} > 6.8$. On the other hand, sulfamethoxazole has two pK_a values including 1.8 ($\text{pK}_{a1} = 1.8$ and $\text{pK}_{a2} = 5.6$). It means that SMX is the positive charged under $\text{pH} = 1.8$ while it is negatively charged

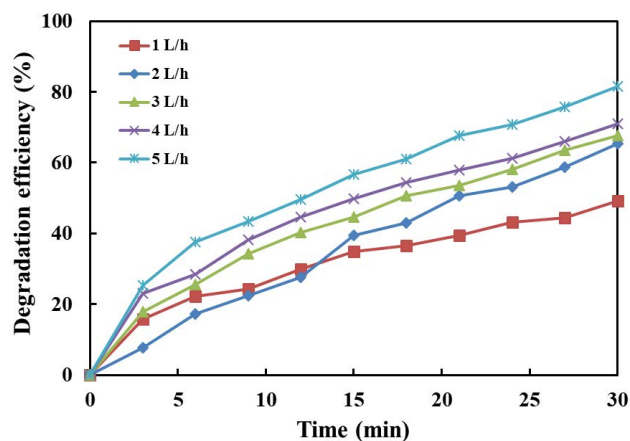


Fig. 13. Effect of ozone gas inlet flow rate on the sulfamethoxazole degradation during the ozonation process. Experimental conditions: $[\text{SMX}]_0$: 20 mg L^{-1} and $\text{pH} = 5$.

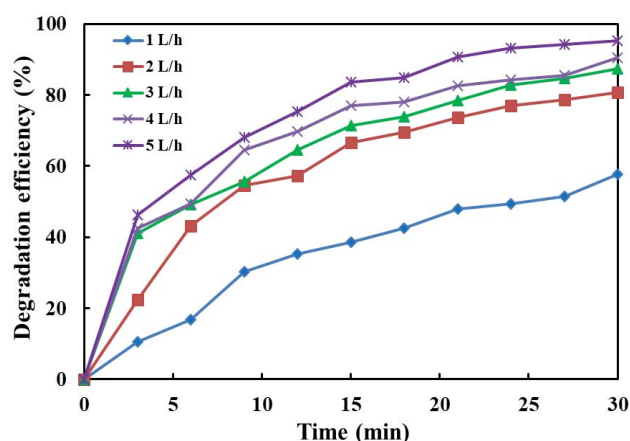


Fig. 14. Effect of ozone gas inlet flow rate on the sulfamethoxazole degradation during photocatalytic ozonation process. Experimental conditions: $[\text{ZnO/MMT}]_0$: 0.1 g L^{-1} ; $[\text{SMX}]_0$: 20 mg L^{-1} ; $\text{pH} = 5$.

when the pH value is higher than 5.6 and it can exist in neutral form (SMX^{\pm}) between $\text{pH} 1.8$ – 5.6 [40]. It is well known that adsorption is a critical factor in photocatalytic ozonation processes.

The highest degradation efficiency at $\text{pH} = 3$ may be attributed to the powerful adsorption of natural SMX molecules onto ZnO/MMT surface through hydrogen bonds. SMX removal reduced from 85.36% ($\text{pH} = 3$) to 80.84% with the increasing pH from 3 to 5. Although the surface charge of catalyst and SMX molecules does not change at these pH values, the observed decrease in SMX removal efficiency probably arises from the increase in aggregation tendency of ZnO/MMT nanoparticles in suspended water resulting in the reduced surface area [57]. As seen from Fig. 15b, percent SMX removal decreased with the increase of solution pH , due to the weak adsorption related to the repulsion effect between SMX molecules and the surface of the catalyst which are positively charged under alkaline conditions.

3.7. Effect of inorganic and organic scavengers

To assay the contribution of the various radical species and holes in the SMX degradation mechanism during photocatalytic ozonation process, which are normally present in water, the experiments were performed using a series of scavengers such as chloride, sulfate, iodide, nitrate and carbonate as inorganic scavengers and t-butanol, $\text{Na}_2\text{-EDTA}$ and chloroform as organic scavengers (Figs. 16 and 17). These substances have different possible effects such as adsorption competition for the active sites on the catalyst surface, reaction with radical species and holes [58]. In this set of experiments, the initial concentration of SMX, the photocatalyst dosage, the salt concentration and the ozone gas inlet flow rate are constant at 20 mg L^{-1} , 0.1 g L^{-1} , 20 mg L^{-1} and 2 L h^{-1} , respectively. As seen from these figures, in the presence all of these quenchers, degradation of SMX by photocatalytic ozonation process is inhibited. Among the inorganic scavengers, NaI displayed the most powerful quenching effect followed by NaNO_3 , NaCl , Na_2CO_3 and Na_2SO_4 . Scavenger effect of SO_4^{2-} ion can be explained that the depositon of this ion on the positively charged catalyst surface via van der Waals forces and hydrogen bonds and/or ligand exchange mechanism resulting the reduced catalyst activity [59]. On the other hand, sulfate ions exhibit

Table 3

SMX degradation rate constants with regression coefficients for the various gas flow rates during ozonation and photocatalytic ozonation processes: $[\text{ZnO/MMT}]_0$: 0.1 g L^{-1} ; $[\text{SMX}]_0$: 20 mg L^{-1} ; $\text{pH} = 5$

Gas inlet Flow rate (L h^{-1})	With catalyst		Without catalyst	
	k_{app} ($\text{mg L}^{-1} \text{ min}^{-1}$)	R^2	k_{app} ($\text{mg L}^{-1} \text{ min}^{-1}$)	R^2
1	0.026	0.9730	0.018	0.9901
2	0.056	0.9832	0.035	0.9896
3	0.058	0.9971	0.033	0.9958
4	0.062	0.9763	0.035	0.9943
5	0.094	0.9916	0.048	0.9871

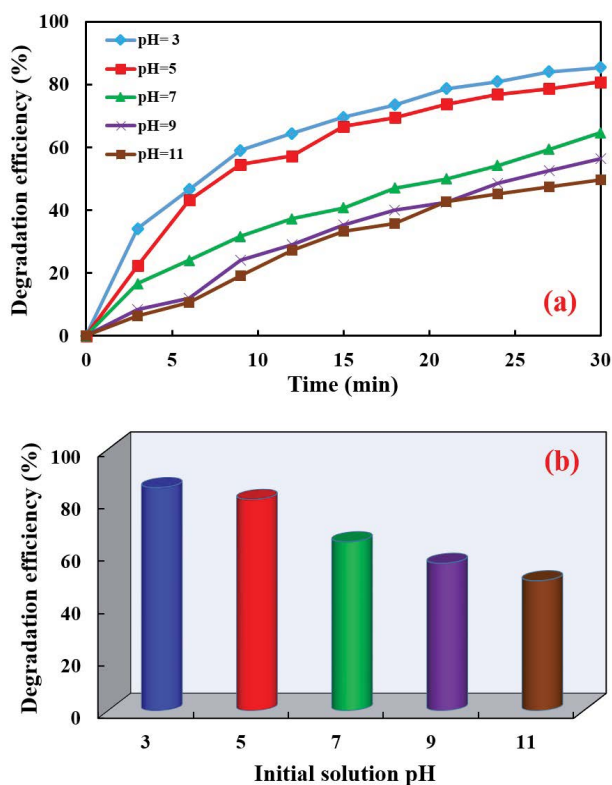
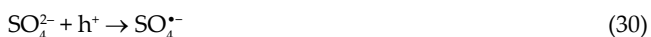


Fig. 15. Effect of initial solution pH on the sulfamethoxazole degradation efficiency during photocatalytic ozonation process (a) at a different time and (b) at 30 min degradation. Experimental conditions: $[SMX]_0 = 20 \text{ mg L}^{-1}$; $[ZnO/MMT]_0 = 0.1 \text{ g L}^{-1}$; ozone gas inlet flow rate = 2 L h^{-1} .

quenching effect on the photogenerated h^+ of ZnO/MMT photocatalyst and produced hydroxyl radicals which cause to generation of less reactive $SO_4^{\cdot-}$ radicals as represented in Eqs. (30) and (31) [60]:



SMX degradation efficiency decreased from 80.84% to 74.31% with the addition of CO_3^{2-} ions of 20 mg L^{-1} , confirming the scavenger effect of carbonate ions. The reaction between hydroxyl radical and carbonate ions produce carbonate radical $CO_3^{\cdot-}$ which has the lower oxidation potential than the hydroxyl radicals and therefore, the degradation efficiency decreases. The possible reactions representing the quenching effect of sodium carbonate can be represented via the following equation [61].



The existence of chloride ion in the oxidation medium can inhibit the oxidation process by quenching the generated hydroxyl radicals as well as the photo-generated h^+ on the photocatalyst through the following probable equations

thus decrease the SMX degradation efficiency from 80.84% to 70.85%.



Percent SMX degradation efficiency reduced from 80.84% to 65.27% with the addition of nitrate ions NO_3^- into the oxidation medium as the scavenger of both hydroxyl radicals and holes [61] confirming the effective role of holes, and hydroxyl radicals in the degradation of SMX by using photocatalytic ozonation process according to the following equations.



Furthermore, the adsorption of SMX molecules on the ZnO/MMT decreased due to the higher adsorption tendencies of NO_3^- ions onto the catalyst. Consequently, it does not cause only a reduction in the utilization efficiency of ZnO/MMT for UV irradiation but also to inhibits the contact of SMX with surface active sites on the ZnO/MMT.

To evaluate the contribution of both photogenerated holes and hydroxyl radicals on the SMX degradation during the photocatalytic ozonation process, KI was added to the reaction medium. In the presence of iodide ions in an aqueous solution, the degradation efficiency of SMX reduced from 80.84% to 29.59% (Fig. 16). It is well known that valence band holes and hydroxyl radicals can easily capture by iodide anions [62,63]. As illustrated in Fig. 16, as a result of the addition of iodide anion, the considerable inhibition of the SMX degradation compared to the other scavengers may be attributed to the excellent role of photoproduced holes and hydroxyl radicals in the degradation phenomena during the photocatalytic ozonation process and stronger scavenging ability of iodide anions.

In addition to the inorganic scavengers, the effect of some organic scavengers, such as t-butanol, chloroform and Na_2 -EDTA was investigated on the SMX degradation during the photocatalytic ozonation process. 1:1 molar ratios of scavengers to SMX were studied. Fig. 17 displays that the addition of t-butanol, chloroform and Na_2 -EDTA and p-benzoquinone caused a remarkable decrease in the degradation efficiency of SMX from 80.84% to 75.59%, 62.74% and 45.87%, respectively.

Fig. 17 illustrates that the SMX degradation via photocatalytic ozonation process was inhibited with the addition of t-BuOH as the hydroxyl radical scavenger, exhibiting the dominant role of $\cdot OH$ radicals in the photocatalytic ozonation process [64]. The considerable reduction in SMX degradation in the presence of chloroform which reacts with the superoxide ion ($O_2^{\cdot-}$) was observed. This result can be an indication that

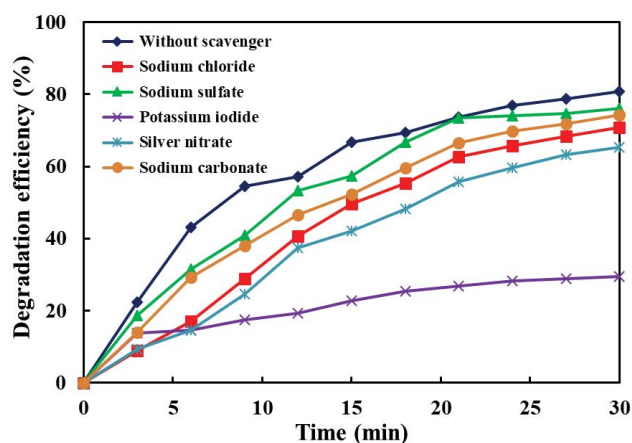


Fig. 16. Effect of different inorganic salts on the sulfamethoxazole degradation under photocatalytic ozonation process. Experimental conditions: $[\text{ZnO/MMT}] = 0.1 \text{ g L}^{-1}$; $[\text{Inorganic salt}]_0 = 20 \text{ mg L}^{-1}$; $[\text{SMX}]_0 = 20 \text{ mg L}^{-1}$; ozone gas inlet flow rate = 2 L h^{-1} ; pH = 5.

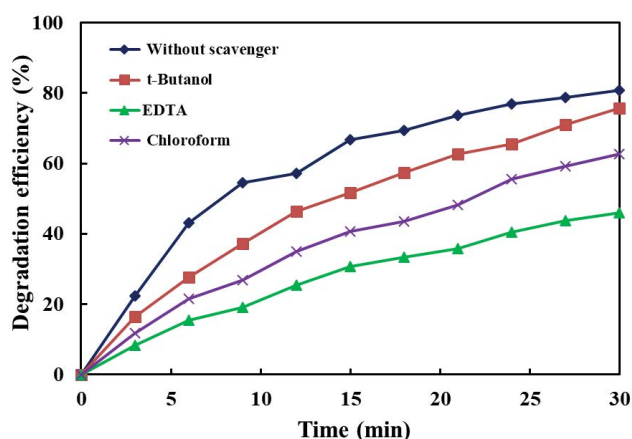


Fig. 17. Effect of different organic salts on the sulfamethoxazole degradation under photocatalytic ozonation process. Experimental conditions: $[\text{ZnO/MMT}] = 0.1 \text{ g L}^{-1}$; $[\text{Salt}]_0 = 20 \text{ mg L}^{-1}$; $[\text{SMX}]_0 = 20 \text{ mg L}^{-1}$; ozone gas inlet flow rate = 2 L h^{-1} ; pH = 5.

O_2^- radicals in aqueous solution have an excellent contribution in the SMX degradation by using photocatalytic ozonation process. EDTA is well-known scavenger of positive holes but it gives very slowly reaction with ozone.

This result obviously reveals the significantly degrading role of photoproducted holes (h^+) in the photocatalytic ozonation of SMX. On the other hand, EDTA has adsorption property on the catalyst surface. Based on these results, it can be concluded that the inhibitory effect of EDTA arises from both its competitive adsorption onto catalyst surface which hinders the synergistic reactions and the consumption of h^+ by EDTA molecules. It should be noted that the percent SMX degradation decreases, but is not totally stopped with the addition of scavengers. This result can be attributed to the contribution of direct ozonation reactions in the SMX degradation [65].

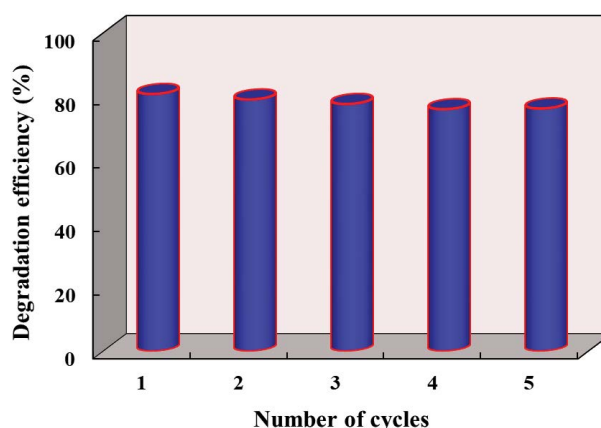


Fig. 18. Reusability of the ZnO/MMT nanocomposite within five consecutive experimental runs at the reaction time of 30 min. Experimental conditions: $[\text{ZnO/MMT}]_0 = 0.1 \text{ g L}^{-1}$; $[\text{SMX}]_0 = 20 \text{ mg L}^{-1}$; pH = 5.

3.8. Reusability of the ZnO/MMT nanocomposite catalyst on the SMX degradation via photocatalytic ozonation process

To evaluate the mechanical and chemical stability of the ZnO/MMT catalyst used in this study, the photocatalytic ozonation experiments were carried out under the same operational conditions. In each of experimental run, the applied ZnO/MMT nanocomposite was separated from the solution by centrifugation, washed with water and dried to use in the next experiment. The results are given in Fig. 18. The obtained results indicated that the slightly change in the SMX degradation efficiency occurred after five runs. The percent SMX degradation efficiency reduced from 80.84% to 76.28% in five photocatalytic ozonation run, approving the stability of ZnO/MMT nanocomposite (Fig. 18).

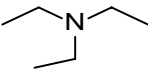
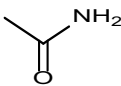
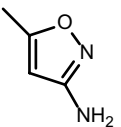
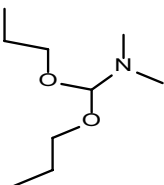
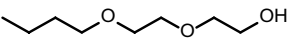
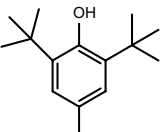
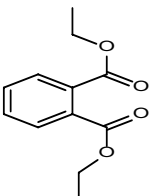
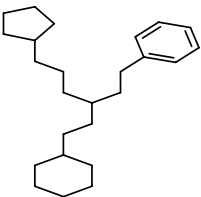
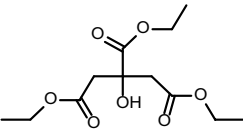
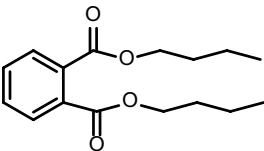
3.9. Analysis of degradation intermediates of SMX during photocatalytic ozonation

During the photocatalytic ozonation process, it was analyzed three times with GC-MS produced by the products after 15 min to reveal the degradation intermediates of sulfamethoxazole [66]. General peaks obtained for the three analysis results were selected and evaluated. The resulting by-products were evaluated by comparing the spectra recorded in the library of mass spectra. The data obtained are given in Table 4.

4. Conclusion

The combination of heterogeneous photocatalysis and ozonation processes accompanied by ZnO/MMT photocatalyst was applied to remove sulfamethoxazole antibiotic from aqueous solution. To prepare ZnO/MMT catalyst, synthesized ZnO nanoparticles was immobilized onto MMT surface. The samples were characterized by the analytical techniques of XRF, XRD, SEM, HR-TEM and N_2 adsorption-desorption. Characterization results confirmed the successful immobilization of ZnO onto MMT surface. The effect

Table 4
Identified by-products during the photocatalytic ozonation of 40 mg L⁻¹ SMX

No.	Compound name	Chemical structure	Retention time (min)	Main fragments
1	Triethylamine		3.19	86.00 (%100.00); 58.00 (%22.30); 101.00 (%18.00); 77.00 (%8.70); 42.00 (%8.10)
2	Acetamide		4.15	59.00 (%100.00); 44.00 (%48.30); 43.00 (%48.36); 42.00 (%25.20); 41.00 (%5.8)
3	3-isoxazolamine, 5-methyl-		5.93	98.00 (%100.00); 55.00 (%49.00); 43.00 (%35.00); 41.00 (%10.20); 42.00 (%9.20)
4	N,N-dimethylformamide dipropyl acetal		6.27	74.00 (%100.00); 116.00 (%56.70); 75.00 (%40.80); 44.00 (%33.70); 73.00 (%30.90)
5	Ethanol, 2-(2-butoxyethoxy)-		7.66	57.00 (%100.00); 45.00 (%89.90); 41.00 (%40.50); 75.00 (%30.00); 44.00 (%26.50)
6	Phenol, 2,6-bis (1,1-dimethylethyl)-4-methyl		12.03	205.00 (%100.00); 220.00 (%24.30); 206.00 (%14.90); 57.00 (%11.80); 145.00 (%11.70)
7	Diethyl phthalate		13.04	149.00 (%100.00); 177.00 (%23.30); 150.00 (%10.90); 44.00 (%10.30); 105.00 (%10.30)
8	Benzene, [3-(2-cyclohexylethyl)-6-cyclopentylhexyl]-		13.87	92.00 (%100.00); 91.00 (%85.20); 83.00 (%43.80); 157.00 (%41.20); 44.00 (%23.30)
9	Triethyl citrate		13.93	157.00 (%100.00); 115.00 (%34.60); 203.00 (%13.70); 43.00 (%12.80); 111.00 (%8.00)
10	1,2-benzenedicarboxylic acid, dibutyl ester		17.22	149.00 (%100.00); 44.00 (%32.50); 57.00 (%17.70); 41.00 (%16.50); 43.00 (%11.00)

of the various operational parameters, such as catalyst dosage, initial SMX concentration, ozone gas flow rate and pH on the SMX degradation efficiency was investigated. The role photo generated radicals and holes and direct ozonation in SMX degradation was understood from the carried out photocatalytic ozonation experiments with the addition of inorganic and organic scavengers into reaction medium. The obtained results for SMX removal with the various processes involving adsorption, ozonation, photolysis, catalytic ozonation, photocatalysis, and photocatalytic ozonation revealed the higher efficiency of photocatalytic ozonation process in SMX degradation. ZnO/MMT catalyst was more efficient compared with ZnO catalyst for SMX removal via photocatalytic ozonation method. The higher efficiency of ZnO/MMT catalyst could be attributed to the effective electron-hole separation as a result of the capturing of photoexcited electrons of ZnO by MMT and to the increased surface area of ZnO/MMT with immobilization. Based on the obtained results from the experiments it can be said that the treatment of wastewaters involving the pharmaceuticals by photocatalytic ozonation process under UV light irradiation accompanied with ZnO/MMT as an excellent photocatalyst is a promising way. And also, this system should be a low-cost, efficient, and nontoxic technology for removal of similar contaminants in wastewaters.

Acknowledgments

The authors would like to express special thanks to the Gümüşhane University and Atatürk University for supports and the East Anatolia High Technology Application and Research Center (DAYTAM) for technical support.

References

- [1] F. Parrino, G. Camera-Roda, V. Loddo, V. Augugliaro, L. Palmisano, Photocatalytic ozonation: maximization of the reaction rate and control of undesired by-products, *Appl. Catal., B*, 178 (2015) 37–43.
- [2] D.H. Quiñones, P.M. Álvarez, A. Rey, F.J. Beltrán, Removal of emerging contaminants from municipal WWTP secondary effluents by solar photocatalytic ozonation. A pilot-scale study, *Sep. Purif. Technol.*, 149 (2015) 132–139.
- [3] M. Fathinia, A.R. Khataee, Photocatalytic ozonation of phenazopyridine using TiO₂ nanoparticles coated on ceramic plates: mechanistic studies, degradation intermediates and ecotoxicological assessments, *Appl. Catal., A*, 491 (2015) 136–154.
- [4] N.F.F. Moreira, C.A. Orge, A.R. Ribeiro, J.L. Faria, O.C. Nunes, M.F.R. Pereira, A.M.T. Silva, Fast mineralization and detoxification of amoxicillin and diclofenac by photocatalytic ozonation and application to an urban wastewater, *Water Res.*, 87 (2015) 87–96.
- [5] M. Mehrjouei, S. Müller, D. Möller, A review on photocatalytic ozonation used for the treatment of water and wastewater, *Chem. Eng. J.*, 263 (2015) 209–219.
- [6] D.H. Quiñones, A. Reya, P.M. Álvarez, F.J. Beltrán, G.L. Puma, Boron doped TiO₂ catalysts for photocatalytic ozonation of aqueous mixtures of common pesticides: Diuron, o-phenylphenol, MCPA and terbuthylazine, *Appl. Catal., B*, 178 (2015) 74–81.
- [7] J. Yin, G. Liao, D. Zhu, P. Lu, L. Li, Photocatalytic ozonation of oxalic acid by g-C₃N₄/graphene composites under simulated solar irradiation, *J. Photochem. Photobiol., A*, 315 (2016) 138–144.
- [8] S. Olivera, C. Hu, G.S. Nagananda, N. Reddy, K. Venkatesh, H.B. Muralidhara, Inamuddin, A.M. Asiri, The adsorptive removal of Cr(VI) ions and antibacterial activity studies on hydrothermally synthesized iron oxide and zinc oxide nanocomposite, *J. Taiwan Inst. Chem. Eng.*, 93 (2018) 342–349.
- [9] M. Saeed, A. Ahmad, R. Boddula, Inamuddin, A. Haq, A. Azhar, Ag@Mn₂O₃: an effective catalyst for photo-degradation of rhodamine B dye, *Environ. Chem. Lett.*, 16 (2018) 287–294.
- [10] M.O. Alfred, M.O. Omorogie, O. Bodede, R. Moodley, A. Ogunlaja, O.G. Adeyemi, C. Günter, A. Taubert, I. Iermak, H. Eckert, I.D.A. Silva, A.S.S. de Camargo, A.J. Motheo, S.M. Clarke, E.I. Unuabonah, Solar-active clay-TiO₂ nanocomposites prepared via biomass assisted synthesis: efficient removal of ampicillin, sulfamethoxazole and artemether from water, *Chem. Eng. J.*, 398 (2020) 125544, doi: 10.1016/j.cej.2020.125544.
- [11] A. Mezni, N.B. Saber, M.M. Ibrahim, M. El-Kemary, A. Aldalbahi, P. Feng, L.S. Smiri, T. Altalhi, Facile synthesis of highly thermally stable TiO₂ photocatalysts, *New J. Chem.*, 41 (2017) 5021–5027.
- [12] J.T. Tsiepe, B.B. Mamba, Inamuddin, A.S. Abd-El-Aziz, A.K. Mishra, Fe₃O₄-β-cyclodextrin-chitosan bionanocomposite for arsenic removal from aqueous solution, *J. Inorg. Organomet. Polym. Mater.*, 28 (2018) 467–480.
- [13] M. Elfiky, N. Salahuddin, A. Matsuda, Green fabrication of 3D hierarchical blossom-like hybrid of peeled montmorillonite-ZnO for in-vitro electrochemical sensing of diltiazem hydrochloride drug, *Mater. Sci. Eng., C*, 111 (2020) 110773, doi: 10.1016/j.msec.2020.110773.
- [14] G. Sharma, A. Kumar, Inamuddin, M. Sood, A.M. Asiri, Fabrication and characterization of polysorbate/ironmolybdo-phosphate nanocomposite: ion exchange properties and pH-responsive drug carrier system for methylcobalamin, *Curr. Anal. Chem.*, 16 (2020) 138–148.
- [15] Y. Jing, L. Li, Q. Zhang, P. Lu, P. Liu, X. Lü, Photocatalytic ozonation of dimethyl phthalate with TiO₂ prepared by a hydrothermal method, *J. Hazard. Mater.*, 189 (2011) 40–47.
- [16] T.B. Horn, F.V. Zerwes, L.T. Kist, Ê.L. Machado, Constructed wetland and photocatalytic ozonation for university sewage treatment, *Ecol. Eng.*, 63 (2014) 134–141.
- [17] D.H. Quiñones, A. Rey, P.M. Álvarez, F.J. Beltrán, P.K. Plucinski, Enhanced activity and reusability of TiO₂ loaded magnetic activated carbon for solar photocatalytic ozonation, *Appl. Catal., B*, 144 (2014) 96–106.
- [18] M. Karaca, M. Kıranşan, S. Karaca, A.R. Khataee, A. Karimi, Sonocatalytic removal of naproxen by synthesized zinc oxide nanoparticles on montmorillonite, *Ultrason. Sonochem.*, 31 (2016) 250–256.
- [19] I. Fatimah, S. Wang, D. Wulandari, ZnO/montmorillonite for photocatalytic and photochemical degradation of methylene blue, *Appl. Clay Sci.*, 53 (2011) 553–560.
- [20] S. Meshram, R. Limaye, S. Ghodke, S. Nigam, S. Sonawane, R. Chikate, Continuous flow photocatalytic reactor using ZnO-bentonite nanocomposite for degradation of phenol, *Chem. Eng. J.*, 172 (2011) 1008–1015.
- [21] P. Raizada, P. Singha, A. Kumar, G. Sharma, B. Pare, S.B. Jonnalagadda, P. Thakur, Solar photocatalytic activity of nano-ZnO supported on activated carbon or brick grain particles: role of adsorption in dye degradation, *Appl. Catal., A*, 486 (2014) 159–169.
- [22] W.G. Xu, S.F. Liu, S.X. Lu, S.Y. Kang, Y. Zhou, H.F. Zhang, Photocatalytic degradation in aqueous solution using quantum-sized ZnO particles supported on sepiolite, *J. Colloid Interface Sci.*, 351 (2010) 210–216.
- [23] M.Y. Ghaly, M.E.M. Ali, L. Österlund, I.A. Khattab, M.I. Badawy, J.Y. Farah, F.M. Zaher, M.N. Al-Maghrabi, ZnO/spiral-shaped glass for solar photocatalytic oxidation of Reactive Red 120, *Arabian J. Chem.*, 10 (2017) 3501–3507.
- [24] J. Ye, X. Li, J. Hong, J. Chen, Q. Fan, Photocatalytic degradation of phenol over ZnO nanosheets immobilized on montmorillonite, *Mater. Sci. Semicond. Process.*, 39 (2015) 17–22.

- [25] P.T. Hang, G.W. Brindley, Methylene blue absorption by clay minerals. Determination of surface areas and cation exchange capacities (clay-organic studies XVIII), *Clays Clay Miner.*, 18 (1970) 203–212.
- [26] M. Kıranşan, A.R. Khataee, S. Karaca, M. Sheydaei, Artificial neural network modeling of photocatalytic removal of a disperse dye using synthesized ZnO nanoparticles on montmorillonite, *Spectrochim. Acta, Part A*, 140 (2015) 465–473.
- [27] D. Chen, Q. Zhu, F. Zhou, X. Deng, F. Li, Synthesis and photocatalytic performances of the TiO₂ pillared montmorillonite, *J. Hazard. Mater.*, 235–236 (2012) 186–193.
- [28] S. Miao, Z. Liu, B. Han, J. Zhang, X. Yu, J. Du, Z. Sun, Synthesis and characterization of TiO₂-montmorillonite nanocomposites and their application for removal of methylene blue, *J. Mater. Chem.*, 16 (2006) 579–584.
- [29] M. Kıranşan, R.D.C. Soltani, A. Hassani, S. Karaca, A.R. Khataee, Preparation of cetyltrimethylammonium bromide modified montmorillonite nanomaterial for adsorption of a textile dye, *J. Taiwan Inst. Chem. Eng.*, 45 (2014) 2565–2577.
- [30] A. Hassani, M. Kıranşan, R.D.C. Soltani, A.R. Khataee, S. Karaca, Optimization of the adsorption of a textile dye onto nanoclay by using central composite design, *Turk. J. Chem.*, 39 (2015) 734–749.
- [31] M. Kıranşan, A.R. Khataee, S. Karaca, M. Sheydaei, Synthesis of zinc oxide nanoparticles on montmorillonite for photocatalytic degradation of Basic yellow 28: effect of parameters and neural network modeling, *Curr. Nanosci.*, 11 (2015) 343–353.
- [32] M.M. Rahman, J. Ahmed, A.M. Asiri, Selective bilirubin sensor fabrication based on doped IAO nanorods for environmental remediation, *New J. Chem.*, 43 (2019) 19298–19307.
- [33] M.J. Rosen, *Surfactants and Interfacial Phenomena*, John Wiley & Sons, New York, 1978.
- [34] M. Tahir, N.S. Amin, Photocatalytic reduction of carbon dioxide with water vapors over montmorillonite modified TiO₂ nanocomposites, *Appl. Catal., B*, 142–143 (2013) 512–522.
- [35] B. Tánhaei, A. Ayati, M. Lahtinen, M. Sillanpää, Preparation and characterization of a novel chitosan/Al₂O₃/magnetite nanoparticles composite adsorbent for kinetic, thermodynamic and isotherm studies of Methyl orange adsorption, *Chem. Eng. J.*, 259 (2015) 1–10.
- [36] G. Li, J. Lan, J. Liu, G. Jiang, Synergistic adsorption of As(V) from aqueous solution onto mesoporous silica decorated orderly with Al₂O₃ and Fe₂O₃ nanoparticles, *J. Colloid Interface Sci.*, 405 (2013) 164–170.
- [37] K. Kočí, L. Matějová, O. Kozák, L. Čapek, V. Valeš, M. Reli, P. Praus, K. Šafařová, A. Kotarba, L. Obalová, ZnS/MMT nanocomposites: the effect of ZnS loading in MMT on the photocatalytic reduction of carbon dioxide, *Appl. Catal., B*, 158–159 (2014) 410–417.
- [38] G. Zhang, X. Ding, F. He, X. Yu, J. Zhou, Y. Hu, J. Xie, Preparation and photocatalytic properties of TiO₂-montmorillonite doped with nitrogen and sulfur, *J. Phys. Chem. Solids*, 69 (2008) 1102–1106.
- [39] A. Mohammad, Inamuddin, S. Hussain, Synthesis and physicochemical characterization of excellent thermally stable and mercury selective organic-inorganic composite cation exchanger polyvinyl alcohol thorium(IV) phosphate, *Desal. Water Treat.*, 57 (2016) 13795–13806.
- [40] O. Ahmed, M.N. Pons, H. Lachheb, A. Houas, O. Zahraa, Degradation of sulfamethoxazole by photocatalysis using supported TiO₂, *Sustainable Environ. Res.*, 24 (2014) 381–387.
- [41] M. Fathinia, A.R. Khataee, S. Aber, A. Naseri, Development of kinetic models for photocatalytic ozonation of phenazopyridine on TiO₂ nanoparticles thin film in a mixed semi-batch photoreactor, *Appl. Catal., B*, 184 (2016) 270–284.
- [42] J. Huang, X. Wang, Z. Pan, X. Li, Y. Ling, L. Li, Efficient degradation of perfluorooctanoic acid (PFOA) by photocatalytic ozonation, *Chem. Eng. J.*, 296 (2016) 329–334.
- [43] F. Parrino, G.C. Roda, V. Loddo, V. Augugliaro, L. Palmisano, Photocatalytic ozonation: maximization of the reaction rate and control of undesired by-products, *Appl. Catal., B*, 178 (2015) 37–43.
- [44] A.R. Khataee, M. Kıranşan, S. Karaca, S. Arefi-Oskoui, Preparation and characterization of ZnO/MMT nanocomposite for photocatalytic ozonation of a disperse dye, *Turk. J. Chem.*, 40 (2016) 546–564.
- [45] V. Augugliaro, M. Litter, L. Palmisano, J. Soria, The combination of heterogeneous photocatalysis with chemical and physical operations: a tool for improving the photoprocess performance, *J. Photochem. Photobiol., C*, 7 (2006) 127–144.
- [46] J. Xiao, Y. Xie, H. Cao, Organic pollutants removal in wastewater by heterogeneous photocatalytic ozonation, *Chemosphere*, 121 (2015) 1–17.
- [47] F.J. Beltran, A. Aguinaco, J.F. Garcia-Araya, Mechanism and kinetics of sulfamethoxazole photocatalytic ozonation in water, *Water Res.*, 43 (2009) 1359–1369.
- [48] M.H. Habibi, M.H. Rahmati, The effect of operational parameters on the photocatalytic degradation of Congo red organic dye using ZnO–CdS core-shell nano-structure, *Spectrochim. Acta, Part A*, 137 (2015) 160–164.
- [49] A.R. Khataee, S. Arefi-Oskoui, M. Fathinia, A. Esmaeili, Y. Hanifehpour, S.W. Joo, N. Hamnabard, Synthesis, characterization and photocatalytic properties of Er-doped PbSe nanoparticles as a visible light-activated photocatalyst, *J. Mol. Catal. A: Chem.*, 398 (2015) 255–267.
- [50] A. Akyol, H.C. Yatmaz, M. Bayramoğlu, Photocatalytic decolorization of Remazol Red RR in aqueous ZnO suspensions, *Appl. Catal., B*, 54 (2004) 19–24.
- [51] N. Daneshvar, D. Salari, A.R. Khataee, Photocatalytic degradation of azo dye acid red 14 in water on ZnO as an alternative catalyst to TiO₂, *J. Photochem. Photobiol., A*, 162 (2004) 317–322.
- [52] S. Sakthivel, B. Neppolian, M.V. Shankar, B. Arabindoo, M. Palanichamy, V. Murugesan, Solar photocatalytic degradation of azo dye: comparison of photocatalytic efficiency of ZnO and TiO₂, *Sol. Energy Mater. Sol. Cells*, 77 (2003) 65–82.
- [53] M. Mehrjouei, S. Müller, D. Möller, Decomposition kinetics of MTBE, ETBE and TAEE in water and wastewater using catalytic and photocatalytic ozonation, *J. Mol. Catal. A: Chem.*, 386 (2014) 61–68.
- [54] A. Aguinaco, F.J. Beltrán, J.F. García-Araya, A. Oropesa, Photocatalytic ozonation to remove the pharmaceutical diclofenac from water: influence of variables, *Chem. Eng. J.*, 189–190 (2012) 275–282.
- [55] W.J. Huang, G.C. Fang, C.C. Wang, A nanometer-ZnO catalyst to enhance the ozonation of 2,4,6-trichlorophenol in water, *Colloids Surf., A*, 260 (2005) 45–51.
- [56] F.J. Beltrán, P. Pocostales, P.M. Alvarez, F. López-Pineiro, Catalysts to improve the abatement of sulfamethoxazole and the resulting organic carbon in water during ozonation, *Appl. Catal., B*, 92 (2009) 262–270.
- [57] P. Gharbani, A. Mehrizad, Heterogeneous catalytic ozonation process for removal of 4-chloro-2-nitrophenol from aqueous solutions, *J. Saudi Chem. Soc.*, 18 (2014) 601–605.
- [58] N.M. Mahmoodi, Photocatalytic ozonation of dyes using multiwalled carbon nanotube, *J. Mol. Catal. A: Chem.*, 366 (2013) 254–260.
- [59] P.S. Yap, T.T. Lim, Effect of aqueous matrix species on synergistic removal of bisphenol-A under solar irradiation using nitrogen-doped TiO₂/AC composite, *Appl. Catal., B*, 101 (2011) 709–717.
- [60] W. Zhang, T. An, M. Cui, G. Sheng, J. Fu, Effects of anions on the photocatalytic and photoelectrocatalytic degradation of reactive dye in a packed-bed reactor, *J. Chem. Technol. Biotechnol.*, 80 (2005) 223–229.
- [61] T. Garoma, S.K. Umamaheshwar, A. Mumper, Removal of sulfadiazine, sulfamethizole, sulfamethoxazole, and sulfathiazole from aqueous solution by ozonation, *Chemosphere*, 79 (2010) 814–820.
- [62] X.V. Doorslaer, P.M. Heynderickx, K. Demeestere, K. Debevere, H.V. Langenhove, J. Dewulf, TiO₂ mediated heterogeneous photocatalytic degradation of moxifloxacin: operational variables and scavenger study, *Appl. Catal., B*, 111–112 (2012) 150–156.

- [63] X. Zhang, D.D. Sun, G. Li, Y. Wang, Investigation of the roles of active oxygen species in photodegradation of azo dye AO7 in TiO₂ photocatalysis illuminated by microwave electrodeless lamp, *J. Photochem. Photobiol., A*, 199 (2008) 311–315.
- [64] F. Qi, W. Chu, B. Xu, Comparison of phenacetin degradation in aqueous solutions by catalytic ozonation with CuFe₂O₄ and its precursor: surface properties, intermediates and reaction mechanisms, *Chem. Eng. J.*, 284 (2016) 28–36.
- [65] J. Sun, X. Yan, K. Lv, S. Sun, K. Deng, D. Du, Photocatalytic degradation pathway for azo dye in TiO₂/UV/O₃ system: hydroxyl radical versus hole, *J. Mol. Catal. A: Chem.*, 367 (2013) 31–37.
- [66] A.R. Khataee, M. Kıranşan, S. Karaca, M. Sheydaei, Photocatalytic ozonation of metronidazole by synthesized zinc oxide nanoparticles immobilized on montmorillonite, *J. Taiwan Inst. Chem. Eng.*, 74 (2017) 196–204.